Galilean-invariant Nosé-Hoover-type thermostats

S. Pieprzyk,[1,*] D. M. Heyes,[2,†] Sz. Maćkowiak,[3,‡] and A. C. Brańka[1,§]
[1]*Institute of Molecular Physics, Polish Academy of Sciences, M. Smoluchowskiego 17, 60-179 Poznań, Poland*
[2]*Department of Physics, Royal Holloway, University of London, Egham, Surrey TW20 0EX United Kingdom*
[3]*Institute of Physics, Poznań University of Technology, Piotrowo 3, 60-965 Poznań, Poland*
(Received 30 January 2015; published 30 March 2015)

A new pairwise Nosé-Hoover type thermostat for molecular dynamics (MD) simulations which is similar in construction to the pair-velocity thermostat of Allen and Schmid, [Mol. Simul. **33**, 21 (2007)] (AS) but is based on the configurational thermostat is proposed and tested. Both thermostats generate the canonical velocity distribution, are Galilean invariant, and conserve linear and angular momentum. The unique feature of the pairwise thermostats is an unconditional conservation of the total angular momentum, which is important for thermalizing isolated systems and those nonequilibrium bulk systems manifesting local rotating currents. These thermostats were benchmarked against the corresponding Nosé-Hoover (NH) and Braga-Travis prescriptions, being based on the kinetic and configurational definitions of temperature, respectively. Some differences between the shear-rate-dependent shear viscosity from Sllod nonequilibrium MD are observed at high shear rates using the different thermostats. The thermostats based on the configurational temperature produced very similar monotically decaying shear viscosity (shear thinning) with increasing shear rate, while the NH method showed discontinuous shear thinning into a string phase, and the AS method produced a continuous increase of viscosity (shear thickening), after a shear thinning region at lower shear rates. Both pairwise additive thermostats are neither purely kinetic nor configurational in definition, and possible directions for further improvement in certain aspects are discussed.

DOI: 10.1103/PhysRevE.91.033312 PACS number(s): 02.70.−c, 05.10.−a, 45.10.−b, 05.20.−y

I. INTRODUCTION

Temperature control in a system of interacting particles has been the subject of intensive investigation over the last few decades. A number of schemes have been proposed, and of them, the deterministic thermostat, in which the equations of motion are modified to cause a system to have an average temperature which is predetermined, appears to be one of the most successful. Under equilibrium thermodynamic conditions the deterministic thermostats allow simulations to be performed in other than isoenergetic or *NVE* conditions. There is continual interest in developing this subject, which is in part driven by the demands of nonequilibrium molecular dynamics (NEMD) simulations in which heat production in the system requires a thermostatting mechanism to achieve steady-state conditions with minimal interference of the system's physical behavior [1,2].

The Nosé-Hoover (NH) thermostat [3,4], which gives the canonical distribution of particle positions and momenta from continuously variable deterministic and time-reversible trajectories, has perhaps proved to be the most popular method among the many constant temperature approaches. A desired temperature in the system is achieved by a feedback mechanism incorporating an additional dynamical variable or frictionlike coefficient. The fluctuations of the variable are driven by the difference between the instantaneous kinetic temperature (defined through the instantaneous kinetic energy) and that corresponding to the target temperature. Many modifications and generalizations based on the Nosé-Hoover scheme have been proposed [5–10].

A second main method of controlling the temperature is the Gaussian thermostat [11,12], in which no additional degree of freedom is involved, and a multiplier as an additional term in the equations of motion for the momentum variables is calculated from a closed expression [1]. Of the two, only the NH thermostat generates the canonical distribution of momenta, but if the initial distribution is canonical, then the Gaussian thermostat preserve it too [1].

The NH and Gaussian thermostats are designed to control the kinetic temperature and therefore are based on the ideal-gas thermometer and the average of the sum of the squares of particle velocities.

Since the seminal paper by Rugh [13], which introduced a statistical mechanical definition of the thermodynamic temperature, measures of temperature other than that based on the kinetic energy have become possible. In fact, there are many phase functions whose average at equilibrium leads to the system temperature. It is clear from a later generalization of Rugh's expression [14,15] that

$$k_B T = \frac{\langle \nabla H \cdot \mathbf{B}(\mathbf{\Gamma}) \rangle}{\langle \nabla \cdot \mathbf{B}(\mathbf{\Gamma}) \rangle}, \tag{1}$$

where $\mathbf{B}$ is a general vector field and $\mathbf{\Gamma} = (\mathbf{q}_1, \ldots, \mathbf{q}_N, \mathbf{p}_1, \ldots, \mathbf{p}_N)$. Other measures of temperature can be obtained by different choices of the vector field, $\mathbf{B}(\mathbf{\Gamma})$. For example, $\mathbf{B} = (0, \ldots, 0, \mathbf{p}_1, \ldots, \mathbf{p}_N)$ gives the conventional kinetic temperature, and $\mathbf{B} = (\mathbf{F}_1, \ldots, \mathbf{F}_N)$ gives an example of the so-called "configurational" temperature, $1/k_B T_{conF} = \langle -\sum_i \nabla_i \cdot \mathbf{F}_i \rangle / \langle \sum_i \mathbf{F}_i^2 \rangle$. The configurational temperature is defined solely in terms of the particle positions or configurational properties of the system.

*pieprzyk@ifmpan.poznan.pl
†david.heyes@rhul.ac.uk
‡szymon.mackowiak@doctorate.put.poznan.pl
§branka@ifmpan.poznan.pl

Different temperature definitions may serve as a foundation for alternative thermostatting schemes. The first deterministic thermostat based on the configurational temperature was invented by Delhommelle and Evans [16]. However, this thermostat does not generate the canonical ensemble, which was corrected subsequently by Braga and Travis (NHBT) [17]. The NHBT configurational thermostat generates the canonical phase-space distribution, and its construction is very much like the NH kinetic temperature thermostat.

The configurational thermostat is expected to be more useful than the kinetic thermostat in the field of NEMD, which generates flow patterns because it does not require prior knowledge of the form of the local streaming velocity [1,2,18]. In the case of the kinetic thermostat one must know or assume *a priori* the streaming velocities at the particle positions to calculate the thermal component of an atom's momentum. This may be problematic, particularly far from equilibrium, where imposing an assumed velocity profile can produce unphysical behavior, e.g., such as the so-called "string phase" [16,18]. It may be expected that temperature control by a configurational temperature is more appropriate for a system of structured molecules, as kinetic thermostats are usually applied to the center-of-mass momenta to avoid the problem of assigning a streaming velocity at atomic sites [16,19]. In their favor, thermostats that control kinetic temperature are more convenient to implement in practice as they need only the momenta variables. Also, the configurational temperature involves the calculation of the derivative of the force, which for more complex force fields may not be a trivial exercise, [18], and cutoff effects can be more pronounced. Also, more recently a number of previously unrecognized features of the configurational thermostat have come to light. For example, Hoover and Hoover [20] observed that there is a rotational contribution to the configurational temperature. Also the NHBT configurational thermostat does not conserve angular momentum, which is discussed later in this report. Although this should not be a problem for systems with periodic boundary conditions, which do not conserve total angular momentum anyway, it may make the thermostat unsuitable for simulations of isolated systems of particles, e.g., clusters or individual structured molecules, by introducing rotation in an uncontrollable way. Furthermore, for some applications Galilean invariance and conservation of both total linear and angular momenta are important. They are, for example, a necessary condition for producing the correct hydrodynamic behavior in dissipative particle dynamics (DPD) simulations [21]. Thermostats which meet these requirements have already been proposed, such as that of Stoyanov and Groot [21], which builds on the previous generalizations by Lowe [22] and Peters [23] of the Andersen thermostat, [24] and the Nosé-Hoover type thermostat proposed by Allen and Schmid [25], which we refer to as "NHASv." A characteristic feature of these thermostats is that they act on pairs of particles rather than single particles. The Stoyanov and Groot thermostat involves a stochastic element and has not been shown to generate the canonical ensemble. The deterministic NHASv thermostat is based on relative velocities of pairs of molecules and generates the canonical distribution of particle positions and momenta. It conserves total linear and angular momentum and is expected to be useful in both DPD and MD simulations. Furthermore as only relative velocities are used to define an instantaneous temperature, the NHASv thermostat may provide a more physically realistic temperature control mechanism for fluid flows and other nonequilibrium situations when compared with the conventional kinetic thermostats which take averages over the whole system.

In this work some less well recognized consequences of the NHBT and NHASv thermostats connected with the angular momentum and fluid flow are investigated. We propose a new deterministic thermostat of the NH type based on pairs of particles and the NHBT equations. The proposed thermostat generates the canonical distribution, is Galilean invariant and conserves both total linear and angular momenta. The new thermostat can be considered to be a counterpart of the NHASv thermostat.

The pairwise NHASv thermostat is described in Sec. II. In Sec. III a pairwise thermostat based on the configurational thermostat is proposed and discussed. The behavior and performance of both pairwise thermostats are analyzed using MD simulations of a few model systems. The simulation details are given in Sec. IV. The main bulk equilibrium properties are studied in Sec. V, and a specific nonequilbrium situation, that of Couette flow, is considered in Sec.VI. The case of small isolated systems is discussed in Sec. VII. In all simulations a comparison is made of the results obtained with the NH and NHBT thermostats. Some possible generalizations of the pairwise NH thermostats are briefly presented in Sec. VIII and conclusions given in Sec. IX.

II. PAIRWISE NOSÉ-HOOVER THERMOSTAT, NHAS*v*

In this work a classical system of N particles in volume V interacting with a pairwise potential, $\phi(r_{ij})$, is considered. The total energy of the system, $H(\mathbf{r},\mathbf{p})$ is the sum of the potential energy, $U(\mathbf{r}) = \sum_{i=1}^{N-1}\sum_{j>i}^{N}\phi(r_{ij})$, and the kinetic energy, $K(\mathbf{p}) = \sum_{i=1}^{N}\mathbf{p}_i^2/2m_i$, where $\mathbf{p}_i$ is the momentum of particle i with mass m_i, at position $\mathbf{r}_i$, and $r_{ij} = \mid \mathbf{r}_{ij} \mid$, where $\mathbf{r}_{ij} = \mathbf{r}_i - \mathbf{r}_j$. The notation $\mathbf{r}$ and $\mathbf{p}$ implies the complete set of coordinates $\{\mathbf{r}_1,\mathbf{r}_2,\ldots,\mathbf{r}_N\}$ and momenta $\{\mathbf{p}_1,\mathbf{p}_2,\ldots,\mathbf{p}_N\}$, respectively. The force acting on particle i is $\mathbf{F}_i = -\nabla_{\mathbf{r}_i}U = \sum_{j\neq i}\mathbf{F}_{ij}$, with the pair forces satisfying Newton's third law, i.e., $\mathbf{F}_{ij} = -\mathbf{F}_{ji}$.

A deterministic, Galilean-invariant thermostat based on relative velocities has been derived by Allen and Schmid [25], which in its final form can be represented by the following equations of motion:

$$\frac{d\mathbf{r}_i}{dt} = \frac{\mathbf{p}_i}{m_i}, \tag{2}$$

$$\frac{d\mathbf{p}_i}{dt} = \mathbf{F}_i - \zeta\boldsymbol{\mathcal{V}}_i, \tag{3}$$

$$\frac{d\zeta}{dt} = \frac{1}{Q_\zeta}\sum_{i}^{N}\left[\frac{\mathbf{p}_i}{m_i}\cdot\boldsymbol{\mathcal{V}}_i - k_BT\nabla_{\mathbf{p}_i}\cdot\boldsymbol{\mathcal{V}}_i\right], \tag{4}$$

where ζ is a dynamical variable or friction-like coefficient and Q_ζ is, as in the Nosé-Hoover method, the thermostat "mass" parameter which determines the extent of coupling of the thermostat to the system. In the above extension of the

NH approach, the quantity $\boldsymbol{\mathcal{V}}_i$ is a function of $(\mathbf{r},\mathbf{p})$, which can be considered to be a generalized particle velocity. In the particular case, $\boldsymbol{\mathcal{V}}_i(\mathbf{r},\mathbf{p}) \equiv \mathbf{p}_i$ the formulas in Eqs. (2)–(4) reduce to the NH scheme. Averaging of the last or the thermostatting equation, Eq. (4) yields the expression for the controlled temperature, $T_{K\mathcal{V}}$,

$$k_B T_{K\mathcal{V}} = \frac{\left\langle \sum_i^N \frac{\mathbf{p}_i}{m_i} \cdot \boldsymbol{\mathcal{V}}_i \right\rangle}{\left\langle \sum_i^N \nabla_{\mathbf{p}_i} \cdot \boldsymbol{\mathcal{V}}_i \right\rangle}, \tag{5}$$

which follows from the general definition of temperature, where $\mathbf{B}(\boldsymbol{\Gamma})$ is set to $(0,0,\ldots,0,\boldsymbol{\mathcal{V}}_1,\boldsymbol{\mathcal{V}}_2,\ldots,\boldsymbol{\mathcal{V}}_N)$. To make the scheme suitable for the DPD simulation, Allen and Schmid wrote the generalized velocity in the pairwise additive form, $\boldsymbol{\mathcal{V}}_i = \sum_{j\neq i} \boldsymbol{\mathcal{V}}_{ij}$ with $\boldsymbol{\mathcal{V}}_{ij} = -\boldsymbol{\mathcal{V}}_{ji}$, where

$$\boldsymbol{\mathcal{V}}_{ij} = (\mathbf{v}_{ij} \cdot \mathbf{W}_{ij})\mathbf{W}_{ij} = W_{ij}^2(\mathbf{v}_{ij} \cdot \hat{\mathbf{r}}_{ij})\hat{\mathbf{r}}_{ij}, \tag{6}$$

$\mathbf{v}_{ij} = \mathbf{v}_i - \mathbf{v}_j$, and $\mathbf{v}_i = \mathbf{p}_i/m_i$ is a particle velocity. W_{ij} is a function of the distance between particles i and j, and its particular form is given below. It can be confirmed that the total linear momentum, $\mathbf{P} = \sum_i \mathbf{p}_i$ and total angular momentum, $\mathbf{L} = \sum_i \mathbf{r}_i \times \mathbf{p}_i$ of the system are conserved without any additional condition; in the NH scheme the conditions $\mathbf{P}(0) = 0$ and $\mathbf{L}(0) = 0$ are required as $\mathbf{P}(t) = \mathbf{P}(0)\exp[-\int_0^t \zeta(t')\,dt']$ and $\mathbf{L}(t) = \mathbf{L}(0)\exp[-\int_0^t \zeta(t')\,dt']$. Also, the central and pairwise additive nature of all forces involved in the scheme implies the dynamics is Galilean invariant.

Additionally, just as in the case of the NH thermostat, a subsidiary equation can be added to the equations of motion which defines the following quantity:

$$H_{\mathrm{NHASv}}(\mathbf{r},\mathbf{p},\zeta,s) = \sum_i \frac{\mathbf{p}^2{}_i}{2m_i} + U(\mathbf{r}) + \frac{1}{2}Q_\zeta \zeta^2 + k_B T ln(s), \tag{7}$$

which is conserved. The subsidiary equation for the NHASv scheme has the form $ds/dt = s\zeta \sum_{i=1}^{N-1}\sum_{j>i}^{N} W_{ij}^2/m_{ij}$, where $m_{ij} = (m_i m_j)/(m_i + m_j)$.

An important feature of the pairwise velocity thermostat is that the phase space function $\rho(\mathbf{r},\mathbf{p},\zeta) \sim \exp[-H(\mathbf{r},\mathbf{p})/k_BT]\exp(-Q_\zeta\zeta^2/2k_BT)$ is a stationary solution of the Liouville equation. It means that the scheme can generate the canonical ensemble [25], just as NH does; however, there is no guarantee that it will for all dynamical systems. In the same paper, the NHASv scheme was tested for a particular form of the pair force typical of that employed in DPD, $\mathbf{W}_{ij} = W_{ij}\hat{\mathbf{r}}_{ij} = w(r_{ij})\hat{\mathbf{r}}_{ij}$, where $w(r < r_c) = 1 - r/r_c$ and is zero otherwise (r_c is the cutoff distance, which in general can be different from the interparticle potential cutoff distance, R_C). It was found that the performance of the scheme in this case is comparable to that of the NH scheme and can be useful in both DPD and MD simulations. Also, because only local relative velocities are used to define an instantaneous temperature it is expected that the NHASv dynamics may provide a more physically realistic way of controlling temperature when there are fluid flows in the modeled system and the property gradients can be large [25].

III. PAIRWISE NHBT THERMOSTAT, NHBTf

The equations of motion of Braga and Travis [17] are

$$\frac{d\mathbf{r}_i}{dt} = \frac{\mathbf{p}_i}{m_i} + \xi\mathbf{F}_i, \tag{8}$$

$$\frac{d\mathbf{p}_i}{dt} = \mathbf{F}_i, \tag{9}$$

$$\frac{d\xi}{dt} = \frac{1}{Q_\xi}\sum_i \left(\mathbf{F}_i^2 + k_B T \nabla_{\mathbf{r}_i} \cdot \mathbf{F}_i\right), \tag{10}$$

which are referred to as the NHBT equations of motion here. They look similar to the NH scheme but are designed to control the configurational rather than the kinetic temperature. The feedback mechanism between the thermostat and the physical system is through the velocity equation, Eq. (8), rather than the force one as in NH, and the dynamical variable ξ is driven by a balance between $\mathbf{F}^2$ and $\nabla \cdot \mathbf{F}$. The balance in this case is through functions which are only particle position dependent. In the extended system the function

$$H_{\mathrm{NHBT}}(\mathbf{r},\mathbf{p},\xi,\chi) = \sum_i \frac{\mathbf{p}^2{}_i}{2m_i} + U(\mathbf{r}) + \frac{1}{2}Q_\xi\xi^2 + k_B T ln(\chi) \tag{11}$$

is a conserved quantity. The time dependence of χ is given by $d\chi/dt = \chi\xi\sum_i \nabla_{\mathbf{r}_i} \cdot \mathbf{F}_i$. The NHBT scheme or configurational thermostat generates the canonical distribution in the physical phase space, $(\mathbf{r},\mathbf{p})$ [17], and its behavior satisfies $d\mathbf{P}/dt = 0$ and $d\mathbf{L}/dt = \xi\sum_i \mathbf{F}_i \times \mathbf{p}_i \neq 0$, which means that the total momentum of the system is conserved but the total angular momentum is not a conserved quantity. In practice, the nonconservation of the total angular momentum is irrelevant for most MD calculations as they are usually performed with the periodic boundary conditions where the $\mathbf{L}$ is not conserved anyway. However, in some cases, such as isolated systems (clusters of particles or macromolecules) or externally driven systems (such as by gravity), the conservation of $\mathbf{L}$ may be essential to preserve. Thus, consequences of the application of the NHBT thermostat to such systems requires clarification, which is one aspect of this work (see Sec. VII).

The conservation of $\mathbf{L}$ can be achieved by a suitable generalization of the NHBT scheme in the form of the following set of equations of motion, which are denoted as "NHBTf":

$$\frac{d\mathbf{r}_i}{dt} = \frac{\mathbf{p}_i}{m_i} + \xi\frac{\mathbf{f}_i}{m_i}, \tag{12}$$

$$\frac{d\mathbf{p}_i}{dt} = \mathbf{F}_i, \tag{13}$$

$$\frac{d\xi}{dt} = \frac{1}{Q_\xi}\sum_i \frac{1}{m_i}(\mathbf{f}_i \cdot \mathbf{F}_i + k_B T \nabla_{\mathbf{r}_i} \cdot \mathbf{f}_i). \tag{14}$$

The function, $\mathbf{f}_i(\mathbf{r},\mathbf{p})$, is in some sense analogous to the $\boldsymbol{\mathcal{V}}_i(\mathbf{r},\mathbf{p})$ function in the NHASv thermostat, with the corresponding pairwise additive property being, $\mathbf{f}_i = \sum_{j\neq i}\mathbf{f}_{ij}$ and $\mathbf{f}_{ij} = -\mathbf{f}_{ji}$.

The expression for the temperature, T_{Cf},

$$k_B T_{Cf} = \frac{\left\langle \sum_i \frac{1}{m_i} \mathbf{f}_i \cdot \mathbf{F}_i \right\rangle}{\left\langle -\sum_i \frac{1}{m_i} \nabla_{\mathbf{r}_i} \cdot \mathbf{f}_i \right\rangle}, \tag{15}$$

follows from Eq. (14) and is a variant of the general temperature definition with the field $\mathbf{B}(\mathbf{\Gamma})$ being $(\mathbf{f}_1, \mathbf{f}_2, \ldots, \mathbf{f}_N, 0, 0, \ldots, 0)$.

In the special case, $\mathbf{f}_i(\mathbf{r},\mathbf{p})/m_i \equiv \mathbf{F}_i$ the NHBTf scheme reduces to the configurational NHBT thermostat, Eqs. (8), (9), and (10). In this special case $k_B T_{Cf}$ reduces to $k_B T_C = \langle \sum_i (\partial U/\partial \mathbf{r}_i)^2 \rangle / \langle \sum_i (\partial^2 U/\partial \mathbf{r}_i^2) \rangle$ which is often denoted in the literature by T_{conF} [14,15,17]. As shown in Appendix A, $d\mathbf{L}/dt = \xi \sum_i \mathbf{f}_i \times \mathbf{p}_i$ is equal to zero if

$$\mathbf{f}_i = \sum_{j \neq i} \mathbf{f}_{ij} = \sum_{j \neq i} (\hat{\mathbf{v}}_{ij} \cdot \mathbf{F}_{ij}) \hat{\mathbf{v}}_{ij} = \sum_{j \neq i} F_{ij} (\hat{\mathbf{v}}_{ij} \cdot \hat{\mathbf{r}}_{ij}) \hat{\mathbf{v}}_{ij}. \tag{16}$$

It is noteworthy that the NHBTf dynamics defined in Eqs. (12), (13), and (14) together with the above $\mathbf{f}_i$ form preserves (as does NHASv) all the main features and symmetries of Newtonian dynamics if the forces between particles are conservative and pairwise additive. These include conservation of total linear momentum and angular momentum, and the mechanical quantity, $\mathbf{G} = t\mathbf{P} - \sum_i m_i \mathbf{r}_i$, which is related to the initial coordinate of the center of mass, $\mathbf{R} = \sum_i m_i \mathbf{r}_i / \sum_i m_i$ (details are given in Appendix A).

It can be shown that the density distribution, $\rho(\mathbf{r},\mathbf{p},\xi) \sim \exp[-H(\mathbf{r},\mathbf{p})/k_B T] \exp(-Q_\xi \xi^2/2k_B T)$ is a stationary solution of the Liouville equation, which means that the scheme generates the canonical ensemble. More specifically, the time average along a trajectory generated by Eqs. (12)–(14) of any phase space variable, $A(\mathbf{r},\mathbf{p})$, of an ergodic system is equal to the canonical ensemble average (or more precisely it is equal to the MD canonical ensemble NVT**PG** for systems in periodic boundary conditions; see Ref. [26]).

As in other NH-type schemes, one extra equation of motion,

$$\frac{d\chi}{dt} = -\chi \xi \sum_i \nabla_{\mathbf{r}_i} \cdot \mathbf{f}_i, \tag{17}$$

allows us to define a quantity of the extended system, denoted by $H_{\mathrm{NHBTf}}(\mathbf{r},\mathbf{p},\xi,\chi)$, which has units of energy and is conserved (see Appendix A). This equation is not needed to generate the evolution of the system. The constant of motion H_{NHBTf} has the same form as H_{NHBT} given in Eq. (11). Some details on the calculation of the $\nabla_{r_i} \cdot \boldsymbol{f}_i$ term and its formula for the LJ interaction are given in Appendix B.

IV. SIMULATIONS

In order to assess the performance of the new pair-particle-based or NHBTf scheme, several tests for equilibrium bulk systems, small clusters, and a fluid undergoing shear flow were performed. Comparisons with two well-established thermostats, the kinetic NH and the configurational NHBT, were made. Calculations were performed also for the NHASv thermostat, which has already been exploited for the "water" DPD model in the work of Allen and Schmid. How it performs for other model pair potentials is investigated. In most of the tests the systems were composed of particles interacting with the Lennard-Jones potential, $\phi(r) = 4\epsilon[(\sigma/r)^{12} - (\sigma/r)^6]$. The calculated quantities are given in conventional pair potential reduced units of ϵ and σ for the energy and length scales, respectively, and time is in units of $\sigma(m/\epsilon)^{1/2}$, temperature in ϵ/k_B, pressure in ϵ/σ^3, and the diffusion coefficient is in $\sigma(\epsilon m)^{1/2}$. The thermostat parameter, Q_ζ or Q_ξ is in the LJ reduced units, $m\sigma^2$ for NH, σ^2/m for NHASv, $(\epsilon^2 m)/\sigma^2$ for NHBT, and $\epsilon^2/(m\sigma^2)$ for NHBTf. For bulk systems periodic boundary conditions were applied and most of the calculations were performed with $N = 864$ particles. The interaction potential cutoff was $R_C = 4$. Isolated clusters of different size composed of $N = 7$, 13, and 33 particles were considered, which are referred to as LJ_7, LJ_{13}, and LJ_{33}, respectively.

The Runge-Kutta algorithm was used to integrate the equations of motion of the clusters or small systems, and the velocity Verlet algorithm which requires only two force calculations per time step was used to integrate equations of the bulk systems with a larger number of particles. The time step was $dt = 0.0005$. After equilibration, the time averages were calculated from simulations of order, 0.5×10^6 time steps for the bulk systems and up to 10 million time steps for the clusters.

For the NH-type thermostats the value of Q_ζ or Q_ξ needs to be chosen carefully. In practice appropriate values can be established by performing preliminary simulations and finding a range where the distribution function of the dynamical variable is Gaussian to a good approximation [27,28]. The known dependence of $Q_\zeta \sim T$ and $Q_\zeta \sim N$ in the case of the NH thermostat [29,30] was also exploited. For the NHASv method a similar dependence is observed. In the case of the NHBT and NHBTf thermostats, the N dependence appears to be $Q_\xi \sim N^2$, which means that for most N and T we have $Q_\xi \gg Q_\zeta$ (in reduced units). In the calculations $Q_\zeta \sim 100$–400 for NH and NHASv, and $Q_\xi \sim 1$–8×10^6 for NHBT and NHBTf were used. For the NH, NHASv, NHBT, and NHBTf thermostats the imposed temperature T is controlled through the suitable feedback, which leads to the expressions for the controlled temperatures, $T_K, T_{K\mathcal{V}}, T_C$, and T_{Cf}, respectively. In the NHASv thermostat, for example, the value of T is introduced into the equation for the variable ζ, which acts as a target temperature. From time averaging of this equation, $k_B T_{K\mathcal{V}}$ as given in Eq. (5) can be calculated, where $T_{K\mathcal{V}}$ is called the "controlled temperature," as it should be equal to T if the scheme is working properly. In the same simulation the averages needed to calculate T_K, T_C, and T_{Cf}, which we call "calculated" or "measured" temperatures, are also accumulated. A measured temperature like any other static average is expected to have a $1/N$ dependence. The controlled temperature is always (within statistical uncertainly) equal to T (by construction), but the measured temperatures may display a different N dependence, which is clearly evident in Fig. 1. Therefore, in simulations with any of these thermostatting schemes, apart from the controlled temperature, the other three temperatures can be calculated, e.g., in the NH scheme the kinetic temperature T_K is the controlled temperature, and the measured three temperatures, i.e., $T_{K\mathcal{V}}, T_{Cf}, T_C$, can be computed from expressions in Eqs. (5) and (15) and $k_B^{-1} \langle \sum_i (\partial U/\partial \mathbf{r}_i)^2 \rangle / \langle \sum_i (\partial^2 U/\partial \mathbf{r}_i^2) \rangle$, respectively. They are all special cases of the statistical mechanical definition of temperature in Eq. (1), which should be the same in the large system

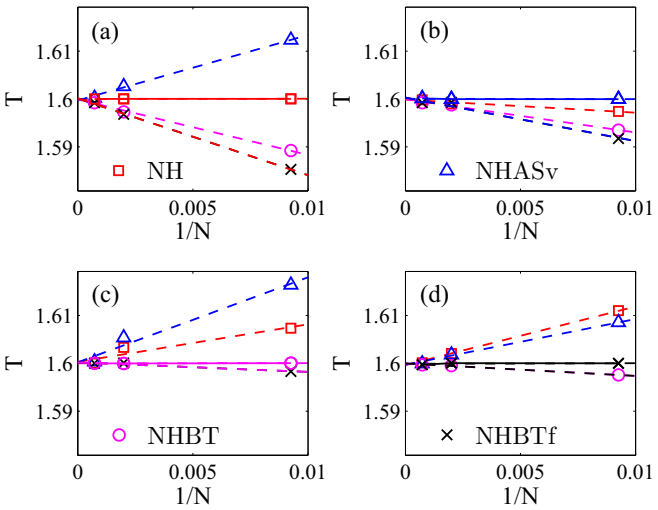

FIG. 1. (Color online) Variation of the controlled (solid lines) and measured (dashed lines) temperature values with system size using the (a) NH, (b) NHASv, (c) NHBT, and (d) NHBTf thermostats. The symbols are results for the LJ fluid at $T = 1.6$, $\rho = 0.3$ for $N = 108,500,1372$. In each subplot $\square,\triangle,\bigcirc$, and $\times$ stand for T_K, T_{Kv}, T_C, and T_{Cf}, respectively. Results for the other simulated state points were tested in the same way: $(T,\rho) = (1.6,0.8442),(1.6,0.5),(0.722,0.8442)$ are similar, and the discrepancy for $N \geqslant 500$ is less than 0.3 %.

limit [14]. In Fig. 1 it is shown that, in fact, the calculated temperatures with the four dynamical schemes are practically the same as the imposed temperature equal for systems for more than about 500 particles in the simulation cell.

V. EQUILIBRIUM BULK SYSTEM PROPERTIES

Some basic thermodynamic properties of several LJ fluid state points were calculated using the four different thermostatting schemes. The results for the potential energy per particle, the pressure, and the heat capacity are given in Table I. The heat capacity was calculated from the energy fluctuation formula.

As may be seen from the table, the averages obtained are identical within the statistical uncertainly of the simulations. Also the uncertainties in the calculated quantities are comparable demonstrating a similar efficiency of the four schemes. Furthermore, the calculated radial distribution functions, $g(r)$, at the same state points were practically insensitive to the thermostatting scheme applied. Thus, as far as structural and thermodynamic properties are concerned, all four thermostats give the same results within the statistical uncertainty of the simulation values.

Some basic time-dependent functions were calculated to examine the effect of the thermostats on dynamical properties. These are the mean-square displacement (MSD), velocity autocorrelation function (vACF), and autocorrelation function of the off-diagonal component of the stress tensor (σACF). As can be seen in Fig. 2, all three functions are unaffected by the choice of the thermostatting scheme.

The diffusion coefficient calculated from the MSD and vACF for a few state points given in Table II are self-consistent. Also, the values of the shear viscosity obtained from the integral of σACF show reasonable agreement. This time the correlation function is based on a many-particle property and therefore shows a greater statistical uncertainty than for the vACF, which is based on a single particle property, for the same simulation time.

An effective thermostatting scheme must steer the system to a target temperature and respond to a change in this temperature so that the calculated temperature follows closely the targeted temperature without any spurious trends or long-lived oscillations. In order to explore this issue, and how well the thermostats perform in this regard, Fig. 3 shows the response of the system to a sudden temperature increase to T_2 followed by its sudden drop to the initial value, T_1, at a later time. The time-accumulated controlled temperature for each type of thermostat is shown in each case. The accumulation starts after each change or pulse of T.

TABLE I. Potential energy, U, pressure P, and heat capacity, C_V of the LJ fluid ($N = 864$) obtained from simulations at four state points using the different thermostatting schemes. The long-range correction, computed with $g(r > R_C) = 1$ is added to U and P. In the last column the data from Johnson *et al.* [31] and from Sadus *et al.* [32] are given. The asterisk indicates that the value was obtained from formulas (7) and (9) in Ref. [31]. The numbers in parentheses are the uncertainties in the final digits.

		NH	NHASv	NHBT	NHBTf	Literature
$T = 0.722$	U	− 6.082(2)	− 6.085(2)	− 6.082(2)	− 6.083(4)	− 6.0883*[a]
$\rho = 0.8442$	P	0.161(5)	0.162(5)	0.161(4)	0.162(5)	0.1550*[a]
	C_V	2.98(47)	2.73(22)	2.64(13)	2.74(21)	–
$T = 1.6$	U	− 5.230(1)	− 5.231(1)	− 5.231(2)	− 5.233(2)	− 5.2508*[a]
$\rho = 0.8442$	P	4.915(3)	4.910(4)	4.909(3)	4.910(3)	4.9112*[a]
	C_V	2.90(47)	2.42(23)	2.38(5)	2.34(14)	2.40[b]
$T = 1.6$	U	− 3.284(2)	− 3.284(2)	− 3.284(2)	− 3.284(2)	− 3.284(2)[a]
$\rho = 0.5$	P	0.547(2)	0.547(1)	0.547(3)	0.551(4)	0.552(3)[a]
	C_V	1.82(24)	2.02(15)	1.89(10)	1.86(10)	1.90[b]
$T = 1.6$	U	− 2.036(3)	− 2.036(3)	− 2.037(3)	− 2.036(3)	− 2.030(6)[a]
$\rho = 0.3$	P	0.278(1)	0.278(1)	0.278(1)	0.278(2)	0.277(1)[a]
	C_V	2.10(28)	2.05(11)	1.89(6)	1.82(23)	1.85[b]

[a]Johnson *et al.* [31].
[b]Sadus *et al.* [32].

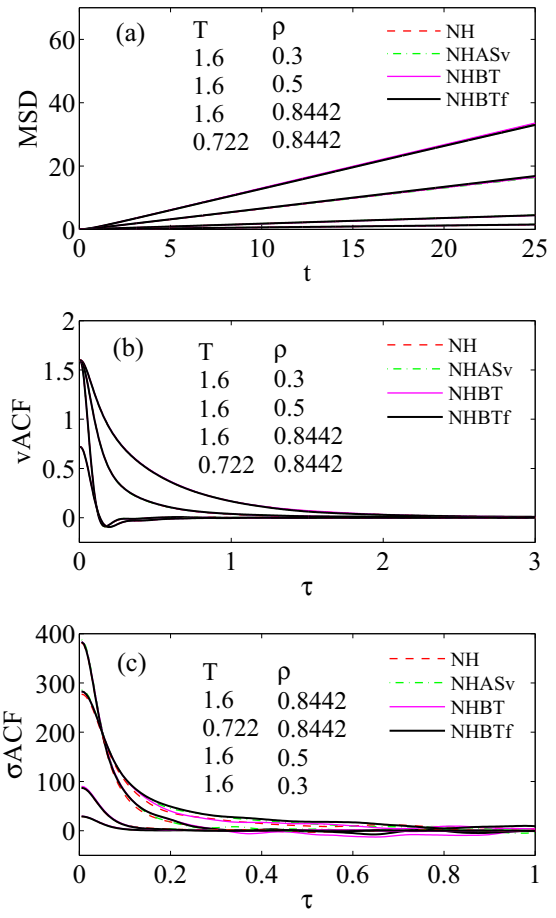

FIG. 2. (Color online) Three types of time-dependent function are shown, namely: (a) the mean-square displacement, MSD, (b) the velocity autocorrelation function vACF, and (c) the off-diagonal pressure tensor autocorrelation function σACF. At each LJ fluid state point (T,ρ), considered the time correlation functions of the four thermostats are practically indistinguishable on the scale of the graphs. The transport coefficients derived from these functions are given in Table II.

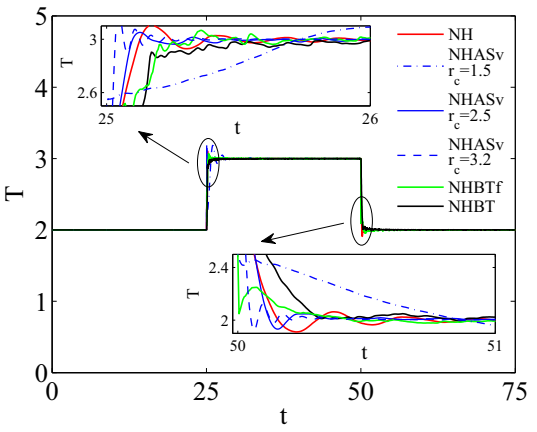

FIG. 3. (Color online) The extent of temperature control where the target temperature is a function of time. Calculations were performed for the LJ fluid ($\rho = 0.8442, N = 256, R_C = 2.5$). The target temperature was changed from $T_1 = 2$ to $T_2 = 3$ at $t = 25$ and returned to T_1 at $t = 50$. The insets show the temperature evolution just after the change of the targeted temperature value. The figure also shows the pair distance cutoff (r_c) dependence of T for the NHASv thermostat.

The calculated temperature quickly responds to the target value after the temperature is changed suddenly for all four thermostats. However, the NH and NHASv schemes show a slight oscillatory behavior just after the temperature step. This effect, seen better in the insets, is sensitive to the Q_ζ value but could not be completely eliminated by tuning this parameter. Also, the value of r_c in the NHASv scheme has an effect on the way the targeted temperature is reached after the pulse. This might have been expected as this parameter regulates the number of particles involved in the thermalization of the system. For small $r_c < R_C$ the heat bath is coupled with the physical system through only a few particles. For simulations, the case where $r_c = R_C$ appears to be an optimal choice.

TABLE II. Transport properties of LJ liquid ($N = 864$) at the same state points as in Table I computed using the different thermostats. The self-diffusion coefficient, D, was calculated from the mean square displacement (MSD) and the velocity autocorrelation function (vACF). The shear viscosity, η, was computed from the corresponding time correlation function [33]. The numbers in parentheses are the uncertainties in the final digits.

		NH	NHASv	NHBT	NHBTf	Woodcock [34]
$T = 0.722$	D_{MSD}	0.030(1)	0.030(1)	0.030(1)	0.030(1)	0.032
$\rho = 0.8442$	$D_{v\mathrm{ACF}}$	0.030(1)	0.030(1)	0.030(1)	0.030(1)	–
	η	2.62(58)	2.60(32)	2.42(70)	2.56(42)	2.535
$T = 1.6$	D_{MSD}	0.090(2)	0.089(2)	0.090(2)	0.090(1)	
$\rho = 0.8442$	$D_{v\mathrm{ACF}}$	0.091(3)	0.089(3)	0.090(3)	0.090(2)	
	η	2.34(35)	2.15(24)	2.19(20)	2.27(50)	
$T = 1.6$	D_{MSD}	0.344(3)	0.343(3)	0.346(2)	0.343(4)	
$\rho = 0.5$	$D_{v\mathrm{ACF}}$	0.350(5)	0.348(6)	0.353(4)	0.347(8)	
	η	0.43(8)	0.41(6)	0.44(6)	0.44(8)	
$T = 1.6$	D_{MSD}	0.682(5)	0.682(6)	0.683(5)	0.679(7)	
$\rho = 0.3$	$D_{v\mathrm{ACF}}$	0.693(4)	0.693(4)	0.695(4)	0.691(4)	
	η	0.18(2)	0.17(2)	0.16(2)	0.18(3)	

To summarize, we note that the simulations carried out for a range of static and dynamic properties of the LJ fluid demonstrate that the two pair thermostats, NHASv and NHBTf, give the same results within the simulation statistical uncertainty as the more established thermostats (NH and NHBT) for key physical properties which specify the thermodynamic and dynamical states of the system. In these specific examples no particular advantages between the pair thermostats have been observed. For equilibrium bulk properties, the NH scheme, being formally the simplest and the easiest one to implement, is the recommended method in our judgment.

VI. NONEQUILIBRIUM PROPERTIES

The behavior of the two pairwise thermostats in the nonequilibrium regime was explored using a WCA model fluid subjected to planar Couette flow. A series of nonequilibrium molecular dynamics (NEMD) simulations was performed with $N = 2048$, $T = 0.722$, and $\rho = 0.8442$, which are the same conditions as those used in previous tests of kinetic and configurational thermostats by Evans and Sarman [16,35]. The Sllod algorithm was used to generate planar Couette flow with shear rates ranging between $\gamma = 0.1$ to 5.0. In the calculations, the time step, $dt = 0.001$, and averages were calculated from production simulations of 1 million steps, after establishing a nonequilibrium steady state of 0.2 million steps. The thermostat "mass" parameters were $400, 0.6, 6 \times 10^6$, and 8×10^6 for the NH, NHASv, NHBT, and NHBTf dynamics, respectively. The shear viscosity was calculated from the ratio of the shear stress to the shear rate: $\eta = -\langle P_{xy} \rangle / \gamma$. The results obtained using the different thermostats are plotted in Fig. 4. The viscosity obtained with the NHBTf thermostat closely follows the results produced with the configurational thermostat (NHBT) at all studied shear rates. The viscosity decreases smoothly with increasing shear rate, without any accompanying shear-induced ordering evident in the snapshots of the particle positions. The shear rate dependence of the viscosity of the NH and NHASv thermostats is similar only to that obtained with NHBTf and NHBT at lower shear rates. At $\gamma \approx 2.4$, a sudden drop in viscosity is clearly visible in the figure for the NH thermostat. The sharp transition in the shear thinning profile is connected with formation of the so-called "string phase," which was much studied in the 1980s (see, for example, Refs. [36,37]). A snapshot of projected particle coordinates on the yz plane shown in the inset indicates that for the NH thermostat there is partial shear-induced ordering along the flow direction for shear rates in excess of *ca.* 2.4 ± 0.1. In the case of the NHASv thermostat, in contrast, the viscosity gradually increases with shear rate within the same γ range. Such "shear thickening" was previously observed in NEMD simulations and might be a consequence of the constant volume condition (see the discussion in Ref. [16,18]). Thus, it may be concluded that the NHASv dynamics cannot be considered as a practical thermostatting scheme for systems away from equilibrium. Although, at lower shear rates the behavior of $\eta(\gamma)$ produced by NHASv is practically the same as that under the NH, NHBT, and NHBTf dynamics. It should be stressed that for nonequilibrium systems the definition of temperature is still problematical, and the nonkinetic energy

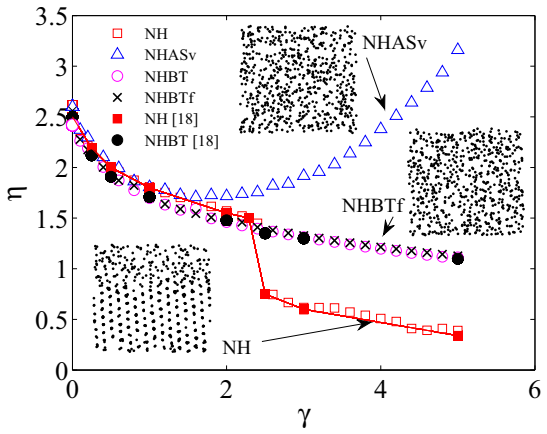

FIG. 4. (Color online) Shear viscosity versus shear rate for the Couette flow simulations of the WCA system at $\rho = 0.8442$ and $T = 0.722$ ($N = 2048$). The results obtained using different deterministic thermostats are presented according to the given symbols, where filled symbols are results from [18]. For *ca.* $\gamma > 2.4$ a sharp decrease of viscosity is visible for the NH thermostat and a more gradual increase in η for the NHASv thermostat. The corresponding snapshot of particle positions in the yz plane (bottom) for the NH thermostat indicates the formation of the string phase. Under NHBT and NHBTf dynamics the viscosity decreases smoothly, and the snapshot of particle positions (top) shows no ordering effect. Such an apparently random pattern of molecular coordinates is also seen for the NHASv dynamics case.

defined thermostats built on the definition given in Eq. (1) assume the thermodynamic definition of temperature exists away from equilibrium (see Chap. 10 in Ref. [1] for further discussion of this issue).

VII. ISOLATED SMALL SYSTEMS

Studies of isolated systems consisting of a small number of particles, such as microclusters, must take into account those specific characteristics which distinguish them from bulk systems. The isolated system generally conserves not only the total energy and total translational momentum but also the total angular momentum. As has previously been demonstrated [38–40] conservation of the angular momentum can considerably influence the properties of this type of system. It causes, for example, the local kinetic temperature of each atom to be inhomogeneous within the cluster. Atoms farther from the center of mass are at a lower temperature than those near the center [41]. Thus, it is necessary in a thermostatting scheme to conserve the total angular momentum and allow for the effects of inhomogeneity of local temperature.

As shown in Secs. II and III, both pairwise thermostats conserve the total angular momentum but the NHBT scheme does not provide conservation of $\mathbf{L}$. Consequently, for example, an atomic cluster at rest [i.e., with $\mathbf{L}(t = 0) = 0$], driven by the NHBT equations starts to rotate in an unpredictable manner, and this unphysical aspect of the NHBT thermostat is illustrated in the bottom set of curves of Fig. 5. This feature makes the NHBT scheme unsuitable for studies of finite-sized systems such as isolated molecules and microclusters.

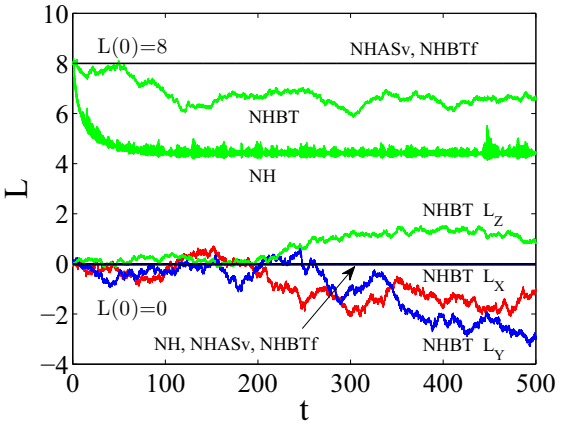

FIG. 5. (Color online) Time evolution of the total angular momentum $\mathbf{L}(t)$, in LJ_{13} cluster at $T = 0.15$. The bottom part of the graph (the curves starting with $L = 0$ at $t = 0$) shows that the initial condition, $\mathbf{L}(0) = 0$, is not preserved by the NHBT dynamics. The upper part of the figure illustrates the situation for an initially rotating cluster with $L_z(0) = 8, L_x(0) = L_y(0) = 0$. In this case only $L_z(t)$ is shown, and, as seen, only NHASv and NHBTf dynamics conserve the initial angular momentum.

In Fig. 6 the local temperature obtained for the small nonrotating LJ clusters with NH, NHASv, and NHBTf dynamics are shown. The local temperature is defined by $T_i^\kappa = 2\langle\kappa_i\rangle/3k_B$, where κ_i is the kinetic energy of ith atom. During the simulations the N particle clusters remain in their stable solid structures. As can be seen in the figure the results produced by the different thermostats are mutually consistent and display the expected behavior of a lower temperature for more distant atoms and a lower inhomogeneity of the local temperature for larger clusters. The results confirm also the

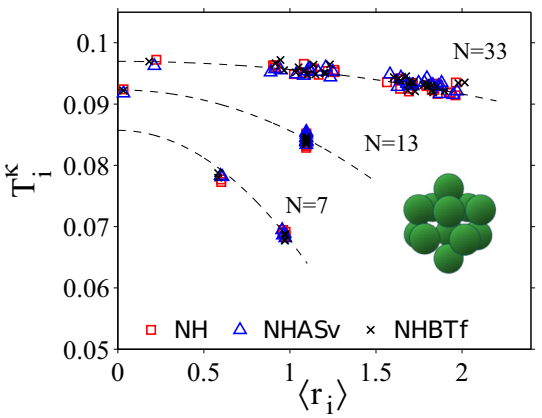

FIG. 6. (Color online) The local kinetic temperature T_i^κ against the atom average distance from the cluster center of mass, $\langle r_i\rangle$. The data were obtained using NH, NHASv, and NHBTf thermostatted dynamics for nonrotating [i.e., $\mathbf{L}(t) = 0$] LJ_7, LJ_{13}, and LJ_{33} clusters at $T = 0.1$. The dashed lines are the theoretical curves from Eq. (18). The atomic positions from the center of mass form groups on the figure, reflecting the coordination shells of the stable solid clusters (seven atoms form a pentagonal bipyramid, 13 atoms form an icosahedron, and 33 atoms a dodecahedron).

validity of the theoretical predictions of Refs. [40,41],

$$T_i^\kappa = \left(1 - \frac{1}{N} - \frac{2m\langle r_i\rangle^2}{3\langle I\rangle}\right) T_K, \tag{18}$$

which are the dashed lines on the figure. In the above expression, $T_K = 2\langle K\rangle/(3N-6)$ is the kinetic temperature, r_i is the atom's distance from the center of mass, and in the derivation a quasi-isotropic shape of the cluster was assumed, $I_x \simeq I_y \simeq I_z = I$ (this assumption is obeyed well for the LJ_7, LJ_{13}, and LJ_{33} clusters). The last term in the expression in Eq. (18) demonstrates how the conservation of total angular momentum affects the kinetic temperature of the atoms.

In the more general case of a cluster with nonzero total angular momentum the evaluation of its kinetic temperature T_K as well as the local temperature T_i^κ requires knowledge of the rotational component of nonrigid systems. There are two methods to deal with this angular momentum conservation problem. There is a special Monte Carlo sampling technique [42] and a partitioning scheme separating vibrational and rotational components of instantaneous kinetic energy [39,43]. The second method, which we exploit in this work, introduces the instantaneous angular velocity $\boldsymbol{\omega}(t)$ defined by the relation $\mathbf{L} = \mathbb{I}(t)\cdot\boldsymbol{\omega}(t)$, where $\mathbb{I}(t)$ is the instantaneous tensor of inertia of the cluster. Knowledge of the fixed vector $\mathbf{L} = \sum_i \mathbf{r}_i \times \mathbf{p}_i = \text{const}$ and calculation at each instant the tensor, $\mathbb{I}(t)$, gives the time evolution of $\boldsymbol{\omega}$ as $\mathbb{I}^{-1}\cdot\mathbf{L}$. The rotational component of the kinetic energy, K_R, is then obtained as $\boldsymbol{\omega}\cdot\mathbf{L}/2$. Thus, a nonrigid cluster at any t is represented via a certain rigid body rotating with angular velocity $\boldsymbol{\omega}(t)$ and having the same $\mathbb{I}(t)$ and $\mathbf{L}$. With this approach the vibrational component $K_V = K - K_R$ or equivalently $K_V = \sum_i^N [\mathbf{p}_i - m_i(\boldsymbol{\omega}\times\mathbf{r}_i)]^2/2m_i$ [39] can now be obtained from which $T_{K_V} = 2 < K_V > /(3N-6)$ (the cluster does not shift, $\mathbf{P} = 0$). From the vibrational part one obtains $\kappa_i = [\mathbf{p}_i - m_i(\boldsymbol{\omega}\times\mathbf{r}_i)]^2/2m_i$, which allows the local kinetic temperature T_i^κ to be determined.

Some results for small rotating clusters driven by the NHBTf and NHASv dynamics are shown in Figs. 7 and 8 for the case of the LJ_{13} cluster where the total angular momentum is $L_x = L_y = 0, L_z = 8$. As shown in Fig. 7 in both cases

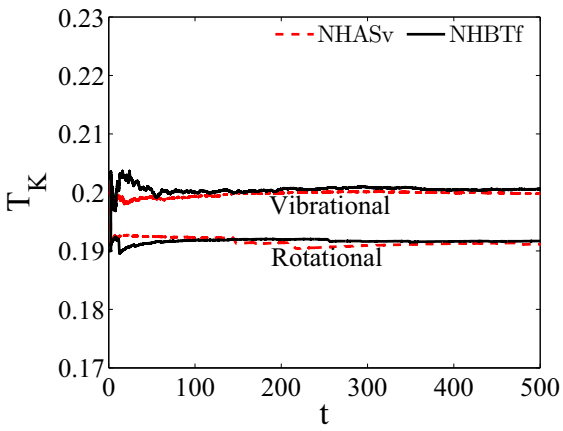

FIG. 7. (Color online) Time evolution of the vibrational (T_{K_V}) and rotational (T_{K_R}) kinetic temperature of a rotating LJ_{13} cluster at $T = 0.2$. The data are generated using the pairwise thermostats, NHASv and NHBTf for $L_z(t) = 8, L_x(t) = L_y(t) = 0$.

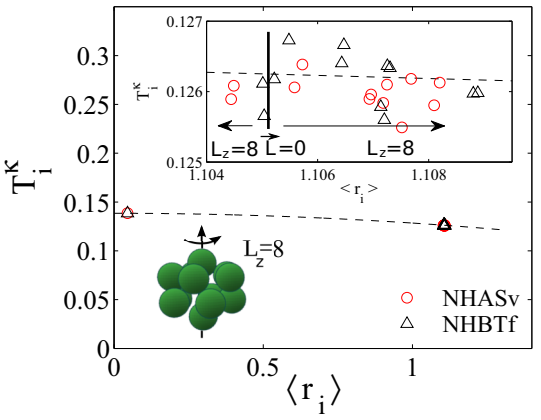

FIG. 8. (Color online) The local kinetic temperature T_i^K of the rotating cluster LJ_{13} at $T = 0.15$. The dashed line is the theoretical curve in Eq. (18). The cluster rotates around the z axis, where $L_z(t) = 8$ and $L_x(t) = L_y(t) = 0$. The rotation causes a slight distortion of the initial spherical top symmetry and consequently, as shown in the inset, a splitting of the outer coordination shell takes place.

the calculated T_{K_V} follows closely the targeted temperature, $T = 0.2$. The corresponding "rotational temperature" $T_{K_R} = 2 < K_R > /(3N - 6)$ indicates almost the same contribution from K_R and K_V to the total kinetic energy in this case.

The calculations performed for rotating LJ_7, LJ_{13}, LJ_{33} clusters demonstrate that the local kinetic temperature displays a very similar r_i, N, and T_K dependence to that observed for nonrotating clusters (i.e., $L = 0$) and can be well represented by the same expression in Eq. (18). As may be seen in Fig. 8 for all i atoms in the cluster $T_i^K(L_z = 8) \approx T_i^K(L = 0)$. Note, however, that the rotation around the z axis causes a slight distortion of the cluster, which becomes an oblate spheroid. This is visible in the inset, which shows splitting of the outer atomic shell. These calculations indicate that even considerable rotation of the cluster has a minor effect on the local kinetic temperature. A more significant effect can

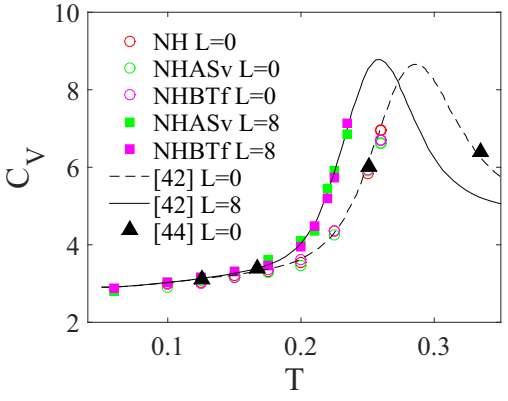

FIG. 9. (Color online) Temperature dependence of heat capacity C_V for the LJ_{13} cluster. The solid line and solid triangles are data from Refs. [42] and [44], respectively. The symbols marked in the figure are results obtained with the deterministic thermostats NH, NHASv, and NHBTf for the nonrotating cluster, and NHASv and NHBTf for the rotating cluster, where $L_z(t) = 8$ and $L_x(t) = L_y(t) = 0$.

be observed in other properties, however, such as the heat capacity. In Fig. 9 the heat capacity C_V versus the temperature for a nonrotating and rotating LJ_{13} clusters is shown. The results produced with the canonical NHBTf and NHASv dynamics reproduce well the data obtained previously with the modified Monte Carlo method [42] and Nosé molecular dynamics [44].

Note that because NHBT dynamics do not conserve angular momentum and the NH dynamics can be exploited only in the particular case of $L = 0$ (see Fig. 5), the pairwise deterministic canonical dynamics (NHBTf, NHASv) are a valuable tool for investigating the dynamical behavior of a rotating cluster at constant temperature.

VIII. EXTENSIONS OF THE PAIRWISE THERMOSTATS

In the NHASv and NHBTf thermostats the precise form of the pairwise functions $\boldsymbol{\mathcal{V}}_i$ and $\mathbf{f}_i$ is determined by $\mathbf{W}_{ij} = w(r_{ij})\hat{\mathbf{r}}_{ij}$ and the interparticle force $\mathbf{F}(r_{ij})$, respectively. It can be shown formally that in both cases these particular forms can be replaced by an arbitrary differentiable function $\mathbf{A}_{ij} = A(r_{ij})\hat{\mathbf{r}}_{ij}$. This presents a potential route to derive a more suitable form for the pairwise functions which could, for example, make NHASv less sensitive to the time step or simplify the calculations of $\nabla_{r_i} \cdot \boldsymbol{f}_i$ (a problem noted in Ref. [18]). Our preliminary calculations indicate that the NHBTf dynamics with $A(r) = n/r^{n+1}$ applied to the LJ fluid yields the same results as in Table I obtained with $A(r) = F(r)$ providing $6 < n < 18$. Thus, from a practical point of view it looks like the $A(r)$ functions should not be substantially different to $F(r)$ or $W(r)$ in analytic form with similar constant and exponent values.

The pairwise thermostats considered in this work are not purely kinetic or configurational thermostats because both $\boldsymbol{\mathcal{V}}_i$ and $\mathbf{f}_i$ depend on the positions and momenta of the particles. The form of the NHASv equations of motion and their performance makes the NHASv thermostat more closely related to the kinetic NH thermostat, however. Similarly the NHBTf thermostat is closer to the configurational NHBT thermostat. These two deterministic thermostats can also be viewed as special cases of the general equations of motion,

$$\frac{d\mathbf{r}_i}{dt} = \frac{\mathbf{p}_i}{m_i} + \xi\frac{\mathbf{f}_i}{m_i}, \tag{19}$$

$$\frac{d\mathbf{p}_i}{dt} = \mathbf{F}_i - \zeta\boldsymbol{\mathcal{V}}_i, \tag{20}$$

$$\frac{d\zeta}{dt} = \frac{1}{Q_\zeta}\sum_i^N\left[\frac{\mathbf{p}_i}{m_i}\cdot\boldsymbol{\mathcal{V}}_i - k_BT\nabla_{\mathbf{p}_i}\cdot\boldsymbol{\mathcal{V}}_i\right], \tag{21}$$

$$\frac{d\xi}{dt} = \frac{1}{Q_\xi}\sum_i\frac{1}{m_i}(\mathbf{f}_i\cdot\mathbf{F}_i + k_BT\nabla_{\mathbf{r}_i}\cdot\mathbf{f}_i). \tag{22}$$

The above set of equations preserves the main features of the NHBTf and NHASv thermostats, in that they produce the canonical distribution, preserve **P**, **L**, and **G**, and are Galilean invariant. This is the form proposed by Kusnezov, Bulgac, and Bauer [6,45], and being a two-variable thermostat is considered to be more efficient in thermalizing *nonmixing*

systems than one-variable thermostats. More investigations along these lines would be required, however, to assess the practical usefulness of such an approach.

IX. CONCLUSIONS

The pairwise NH-type thermostat, NHBTf, proposed in this work extends the methodology of deterministic equations of motion in generating a canonical distribution. In contrast to some other widely used schemes, the NHBTf thermostat involves pairs of particles. This general approach was used recently by Allen and Schmid to formulate the pair velocity thermostat, denoted here by "NHASv," in the context of the DPD simulations. Both pairwise thermostats generate the canonical distribution, are Galilean invariant, and conserve all the basic properties of linear momentum, angular momentum, total energy of the extended system, and the center of mass. In this sense the pairwise scheme seems be the most appropriate of the deterministic thermostat schemes in generating canonical dynamics which are as close to Newtonian dynamics as can be achieved currently.

In this work in a number of test calculations the practical attributes of the pairwise thermostats were studied and compared with the kinetic NH and configurational NHBT thermostats. It was demonstrated that a valuable and unique feature of the pairwise thermostats is their unconditional conservation of the total angular momentum. This property allows a new pairwise NH-type thermostat to be proposed and tested for various properties of rotating isolated systems and for bulk systems where a small part of the system executes concerted rotational motion. As far as equilibrium bulk systems are concerned the pairwise thermostats offer no practical advantages over the currently widely used thermostats (especially the Nosé-Hoover one). In fact, their efficiency is lower than the NH method owing to the more computationally demanding calculations of the thermostat functions (i.e., $\mathbf{f}_i$ or $\boldsymbol{\mathcal{V}}_i$). To some extent the problem of simplifying the $\nabla_{r_i} \cdot \boldsymbol{f}_i$ term in the NHBTf thermostat equations may be solved by exploiting the nonuniqueness of the $W(r)$ and $\mathbf{f}_i$ functions.

Differences between the four thermostats considered become evident at large shear rates in Sllod Couette flow NEMD simulations. The Braga-Travis (NHBT) thermostat and the pairwise extension of it (NHBTf) produce a monotonically decreasing viscosity with increasing shear rate, which maintains a disordered liquid-like internal structure throughout. The Nosé-Hoover thermostat produces discontinuous shear thinning and in parallel the formation of the string phase. The NHASv thermostat exhibits a transition from shear thinning to shear thickening at high shear rate. It may be no coincidence that the NHASv equations of motion bear some similarity to a Stokesian dynamics (SD) model, which also showed continuous shear thickening [46–48]. The SD equations of motion incorporate a contribution to the force on the particle involving the pair velocities (in that case to represent the lubrication interaction between colloidal particles). Shear thickening can be associated with the formation of jammed cluster of rapidly growing dimensions, which it appears from these studies are more likely to develop with the locally more "responsive" NHASv thermostat than the other pairwise thermostat (NHBTf), which acts on the velocity rather than the acceleration of the particle.

It is worth noting that the pairwise thermostats considered here are in fact neither purely kinetic (as is the NH method) nor purely configurational (like the NHBT method). They can be considered to be special cases of more general prescription and set of equations encapsulated in Eqs. (19)–(22), which might provide a pathway to make future improvements.

The pairwise thermostats will have an advantage in the molecular simulation of bulk polyatomic molecular systems and isolated clusters, as the rotation of the body can have a significant influence on the structural, vibrational, and thermodynamic properties of the system (an example of this influence can be seen in Fig. 9). Evaporation [49] and nucleation [50] processes, the onset of microturbulence in liquids [51], and cluster collision dynamics [43,52] are areas of possible specific application of the pairwise thermostats. Almost 20 years ago a Monte Carlo sampling method was proposed to deal with the rotating cluster problem [42]. The pairwise thermostats are the first deterministic counterpart of this MC method, which additionally allows us to explore the dynamical (time-dependent) properties of rotating clusters. Finally, the pair thermostat may be useful for studying very dilute systems (even when there are periodic boundary conditions) such as a high-temperature gas phase composed of nonspherical particles (or their mixtures) in which the molecules spend a relatively large period of time performing ballistic motion between collisions.

ACKNOWLEDGMENTS

The work has been supported partially by the Polish National Science Center grant DEC-2012/05/B/ST3/03255. Sz.M.'s contribution to this work was financially supported within the project POKL.04.03.00-00-259/12, EU Human Capital Operational Programme.

APPENDIX A: CONSTANTS OF MOTION OF THE NHBTf DYNAMICS

In this Appendix the conservation of four quantities in the NHBTf dynamics is shown: total linear and angular momentum, pseudoenergy, and the center-of-mass-related quantity $\mathbf{G}$.

1. Total linear momentum

The conservation of total momentum, $\mathbf{P} = \sum_i \mathbf{p}_i$, in the NHBTf scheme follows directly from Eq. (13) and the pairwise additive form of forces $\mathbf{F}_{ij} = -\mathbf{F}_{ji}$:

$$\frac{d\mathbf{P}}{dt} = \frac{d}{dt}\sum_i \mathbf{p}_i = \sum_i \frac{d}{dt}\mathbf{p}_i = \sum_i \mathbf{F}_i = \sum_{i\neq j} \mathbf{F}_{ij} = 0. \tag{A1}$$

2. Total angular momentum

In order to prove that the total angular momentum $\mathbf{L} = \sum_i \mathbf{L}_i = \sum_i \mathbf{r}_i \times \mathbf{p}_i$ is conserved or $\mathbf{L} = \text{const}$ we show that

$d\mathbf{L}/dt = 0$. Taking into account Eqs. (12) and (13) and $\sum_i \mathbf{p}_i \times \mathbf{p}_i/m_i = 0$, $\sum_i \mathbf{r}_i \times \mathbf{F}_i = 0$ it follows that

$$\begin{aligned}\frac{d\mathbf{L}}{dt} &= \sum_i \frac{d\mathbf{r}_i}{dt} \times \mathbf{p}_i + \sum_i \mathbf{r}_i \times \frac{d\mathbf{p}_i}{dt} \\ &= \sum_i \frac{\mathbf{p}_i}{m_i} \times \mathbf{p}_i + \xi \sum_i \frac{\mathbf{f}_i}{m_i} \times \mathbf{p}_i + \sum_i \mathbf{r}_i \times \mathbf{F}_i \\ &= \xi \sum_i \frac{\mathbf{f}_i}{m_i} \times \mathbf{p}_i. \end{aligned} \tag{A2}$$

Next, the pairwise function $\mathbf{f}_i$ is substituted,

$$\begin{aligned}\sum_i \frac{\mathbf{f}_i}{m_i} \times \mathbf{p}_i &= \sum_i \left[\sum_{j\neq i}^{N} (\mathbf{v}_{ij} \cdot \mathbf{F}_{ij}) \frac{\mathbf{v}_{ij}}{v_{ij}^2} \right] \times \mathbf{v}_i \\ &= \left[(\mathbf{v}_{12} \cdot \mathbf{F}_{12}) \frac{\mathbf{v}_{12}}{v_{12}^2} + (\mathbf{v}_{13} \cdot \mathbf{F}_{13}) \frac{\mathbf{v}_{13}}{v_{13}^2} + \cdots + (\mathbf{v}_{1N} \cdot \mathbf{F}_{1N}) \frac{\mathbf{v}_{1N}}{v_{1N}^2} \right] \times \mathbf{v}_1 \\ &\quad + \left[(\mathbf{v}_{21} \cdot \mathbf{F}_{21}) \frac{\mathbf{v}_{21}}{v_{21}^2} + (\mathbf{v}_{23} \cdot \mathbf{F}_{23}) \frac{\mathbf{v}_{23}}{v_{23}^2} + \cdots + (\mathbf{v}_{2N} \cdot \mathbf{F}_{2N}) \frac{\mathbf{v}_{2N}}{v_{2N}^2} \right] \times \mathbf{v}_2 \\ &\quad + \cdots + \left[(\mathbf{v}_{N1} \cdot \mathbf{F}_{N1}) \frac{\mathbf{v}_{N1}}{v_{N1}^2} + (\mathbf{v}_{N2} \cdot \mathbf{F}_{N2}) \frac{\mathbf{v}_{N2}}{v_{N2}^2} + \cdots + (\mathbf{v}_{N(N-1)} \cdot \mathbf{F}_{N(N-1)}) \frac{\mathbf{v}_{N(N-1)}}{v_{N(N-1)}^2} \right] \times \mathbf{v}_N. \end{aligned} \tag{A3}$$

In this sum for each term $((\mathbf{v}_{ij} \cdot \mathbf{F}_{ij})\mathbf{v}_{ij}/v_{ij}^2) \times \mathbf{v}_i$ there exists the corresponding term $[(\mathbf{v}_{ji} \cdot \mathbf{F}_{ji})\mathbf{v}_{ji}/v_{ji}^2] \times \mathbf{v}_j$. Because $\mathbf{v}_{ij} = -\mathbf{v}_{ji}$ and $\mathbf{F}_{ij} = -\mathbf{F}_{ji}$, their sum is $(\mathbf{v}_{ij} \cdot \mathbf{F}_{ij})(\mathbf{v}_{ij} \times \mathbf{v}_{ij})/v_{ij}^2 = 0$, which means that the entire sum, $\sum_i \mathbf{f}_i \times \mathbf{p}_i/m_i = 0$, and consequently $\mathbf{L} = \text{const}$.

3. The quantity H_{NHBTf}

The conservation of $H_{\text{NHBTf}} = \sum_i \mathbf{p}_i^2/2m + U(\mathbf{r}) + Q_\xi \xi^2/2 + k_B T \ln(\chi)$ follows from the following straightforward algebra:

$$\begin{aligned}\frac{dH_{\text{NHBTf}}}{dt} &= \sum_i \frac{\mathbf{p}_i}{m_i} \cdot \frac{d\mathbf{p}_i}{dt} - \sum_i \mathbf{F}_i \cdot \frac{d\mathbf{r}_i}{dt} + Q_\xi \xi \frac{d\xi}{dt} + k_B T \frac{1}{\chi} \frac{d\chi}{dt} \\ &= \sum_i \frac{\mathbf{p}_i}{m} \cdot \mathbf{F}_i - \sum_i \mathbf{F}_i \cdot \frac{\mathbf{p}_i}{m_i} - \xi \sum_i \mathbf{F}_i \cdot \frac{\mathbf{f}_i}{m_i} + \xi \left[\sum_i \mathbf{F}_i \cdot \frac{\mathbf{f}_i}{m_i} + k_B T \sum_i \frac{1}{m_i} \frac{\partial \mathbf{f}_i}{\partial \mathbf{r}_i} \right] - k_B T \xi \sum_i \frac{1}{m_i} \frac{\partial \mathbf{f}_i}{\partial \mathbf{r}_i} \\ &= \sum_i \frac{\mathbf{p}_i}{m} \cdot \mathbf{F}_i - \sum_i \mathbf{F}_i \cdot \frac{\mathbf{p}_i}{m_i} - \xi \sum_i \mathbf{F}_i \cdot \frac{\mathbf{f}_i}{m_i} + \xi \sum_i \mathbf{F}_i \cdot \frac{\mathbf{f}_i}{m_i} + k_B T \xi \sum_i \frac{1}{m_i} \frac{\partial \mathbf{f}_i}{\partial \mathbf{r}_i} - k_B T \xi \sum_i \frac{1}{m_i} \frac{\partial \mathbf{f}_i}{\partial \mathbf{r}_i} = 0. \end{aligned} \tag{A4}$$

In the last expression the terms cancel in pairs for arbitrary $\mathbf{f}_i$.

4. The quantity G

In the NHBTf dynamics in addition to the "energy," the total linear and angular momentum, the quantity, $\mathbf{G} = \mathbf{P}t - \sum m_i \mathbf{r}_i$, is also a constant of motion. This can be proved by noting first that the sum, $\sum_i \mathbf{f}_i = \sum_i \sum_{j\neq i}^{N} (\mathbf{v}_{ij} \cdot \mathbf{F}_{ij})\mathbf{v}_{ij}/v_{ij}^2 = 0$, which follows directly from the property $(\mathbf{v}_{ij} \cdot \mathbf{F}_{ij})\mathbf{v}_{ij} = -(\mathbf{v}_{ji} \cdot \mathbf{F}_{ji})\mathbf{v}_{ji}$. This sum is simply related to the time derivative of the quantity $\mathbf{G}$, through

$$\frac{d\mathbf{G}}{dt} = \frac{d\mathbf{P}}{dt} t + \mathbf{P} - \sum_i m_i \frac{d\mathbf{r}_i}{dt} = \mathbf{P} - \sum_i \mathbf{p}_i - \sum_i \xi \mathbf{f}_i = -\xi \sum_i \mathbf{f}_i, \tag{A5}$$

where in the calculations the conservation of the total momentum $\mathbf{P} = \sum_i \mathbf{p}_i = \text{const}$ was used. Thus, $d\mathbf{G}/dt = 0$ and $\mathbf{G} = \text{const}$. In the situation when the total momentum, $\mathbf{P} = 0$, the center of mass of the system remains constant with time.

APPENDIX B: CALCULATION OF $\nabla_{\mathbf{r}_i} \cdot \mathbf{f}_i$

The NHBTf dynamics involve the calculation of the derivative of the $\mathbf{f}_i$ function. In general the derivation of the analytical expression for this quantity may not be a straightforward exercise as it is a similar problem to the calculation of the configurational Laplacian of the potential energy in the NHBT scheme [18]. In this appendix the expression for a pairwise additive potential is derived.

Writing,

$$\mathbf{f}_i = \sum_{j\neq i}^{N} (\hat{\mathbf{v}}_{ij} \cdot \mathbf{F}_{ij})\hat{\mathbf{v}}_{ij} = \sum_{j\neq i}^{N} \alpha_{ij}\hat{\mathbf{v}}_{ij}, \tag{B1}$$

where

$$\alpha_{ij} = \hat{\mathbf{v}}_{ij} \cdot \mathbf{F}_{ij}, \tag{B2}$$

we have

$$\nabla_{\mathbf{r}_i} \cdot \mathbf{f}_i = \nabla_{\mathbf{r}_i} \cdot \sum_{j\neq i}^{N} \alpha_{ij}\hat{\mathbf{v}}_{ij} = \sum_{j\neq i}^{N} \nabla_{\mathbf{r}_i} \cdot \alpha_{ij}\hat{\mathbf{v}}_{ij} = \sum_{j\neq i}^{N} (\nabla\alpha_{ij} \cdot \hat{\mathbf{v}}_{ij} + \alpha_{ij}\nabla \cdot \hat{\mathbf{v}}_{ij}) = \sum_{j\neq i}^{N} \nabla\alpha_{ij} \cdot \hat{\mathbf{v}}_{ij}. \tag{B3}$$

In the calculation of $\nabla\alpha_{ij} = \nabla(\hat{\mathbf{v}}_{ij} \cdot \mathbf{F}_{ij})$ the vector identity

$$\nabla(\mathbf{A} \cdot \mathbf{B}) = \mathbf{A} \cdot \nabla\mathbf{B} + \mathbf{B} \cdot \nabla\mathbf{A} + \mathbf{A} \times (\nabla \times \mathbf{B}) + \mathbf{B} \times (\nabla \times \mathbf{A}) \tag{B4}$$

where $\mathbf{A}$,$\mathbf{B}$ are arbitrary vectors, and $\nabla\mathbf{B}$,$\nabla\mathbf{A}$ are dyads, can be exploited.

Thus,

$$\nabla(\mathbf{v} \cdot \mathbf{F}) = \mathbf{v} \cdot \nabla\mathbf{F} + \mathbf{F} \cdot \nabla\mathbf{v} + \mathbf{v} \times (\nabla \times \mathbf{F}) + \mathbf{F} \times (\nabla \times \mathbf{v}), \tag{B5}$$

where for clarity the indices are omitted. Because $\nabla\mathbf{v} = 0$, $\nabla \times \mathbf{F} = 0$, and $\nabla \times \mathbf{v} = 0$, the last three terms are zero, and thus

$$\nabla(\mathbf{v} \cdot \mathbf{F}) = \mathbf{v} \cdot \nabla\mathbf{F}. \tag{B6}$$

We calculate now the expression

$$\begin{aligned}
\frac{1}{v^2}\mathbf{v} \cdot (\mathbf{v} \cdot \nabla\mathbf{F}) &= \frac{1}{v^2}(\hat{\mathbf{x}}v_x + \hat{\mathbf{y}}v_y + \hat{\mathbf{z}}v_z) \cdot (\mathbf{v} \cdot \nabla\mathbf{F}) \\
&= \frac{1}{v^2}\left[v_x\left(v_x\frac{\partial F_x}{\partial x} + v_y\frac{\partial F_x}{\partial y} + v_z\frac{\partial F_x}{\partial z}\right) + v_y\left(v_x\frac{\partial F_y}{\partial x} + v_y\frac{\partial F_y}{\partial y} + v_z\frac{\partial F_y}{\partial z}\right)\right. \\
&\quad \left. + v_z\left(v_x\frac{\partial F_z}{\partial x} + v_y\frac{\partial F_z}{\partial y} + v_z\frac{\partial F_z}{\partial z}\right)\right]
\end{aligned} \tag{B7}$$

which in terms of the potential energy has the following form:

$$\begin{aligned}
\frac{1}{v^2}\mathbf{v} \cdot (\mathbf{v} \cdot \nabla\mathbf{F}) &= -\frac{1}{v^2}\left[v_x\left(v_x\frac{\partial^2 U}{\partial x^2} + v_y\frac{\partial^2 U}{\partial x\partial y} + v_z\frac{\partial^2 U}{\partial x\partial z}\right) + v_y\left(v_x\frac{\partial^2 U}{\partial y\partial x} + v_y\frac{\partial^2 U}{\partial y^2} + v_z\frac{\partial^2 U}{\partial y\partial z}\right)\right. \\
&\quad \left. + v_z\left(v_x\frac{\partial^2 U}{\partial z\partial x} + v_y\frac{\partial^2 U}{\partial z\partial y} + v_z\frac{\partial^2 U}{\partial z^2}\right)\right] \\
&= -\frac{1}{v^2}\left[v_x\frac{\partial}{\partial x}\left(v_x\frac{\partial}{\partial x} + v_y\frac{\partial}{\partial y} + v_z\frac{\partial}{\partial z}\right) + v_y\frac{\partial}{\partial y}\left(v_x\frac{\partial}{\partial x} + v_y\frac{\partial}{\partial y} + v_z\frac{\partial}{\partial z}\right)\right. \\
&\quad \left. + v_z\frac{\partial}{\partial z}\left(v_x\frac{\partial}{\partial x} + v_y\frac{\partial}{\partial y} + v_z\frac{\partial}{\partial z}\right)\right]U \\
&= -\frac{1}{v^2}\left(v_x\frac{\partial}{\partial x} + v_y\frac{\partial}{\partial y} + v_z\frac{\partial}{\partial z}\right)\left(v_x\frac{\partial}{\partial x} + v_y\frac{\partial}{\partial y} + v_z\frac{\partial}{\partial z}\right)U \\
&= -\frac{1}{v^2}(\mathbf{v} \cdot \nabla)(\mathbf{v} \cdot \nabla)U = -\frac{1}{v^2}(\mathbf{v} \cdot \nabla)^2 U,
\end{aligned} \tag{B8}$$

from which it follows finally that

$$\begin{aligned}
\nabla_{\mathbf{r}_i} \cdot \mathbf{f}_i &= \nabla_{\mathbf{r}_i} \cdot \sum_{j\neq i}^{N} (\hat{\mathbf{v}}_{ij} \cdot \mathbf{F}_{ij})\hat{\mathbf{v}}_{ij} = \sum_{j\neq i}^{N} \nabla_{\mathbf{r}_i} \cdot (\hat{\mathbf{v}}_{ij} \cdot \mathbf{F}_{ij})\hat{\mathbf{v}}_{ij} \\
&= -\sum_{j\neq i}^{N} \frac{1}{v_{ij}^2}(\mathbf{v}_{ij} \cdot \nabla)^2 U = -\sum_{j\neq i}^{N} (\hat{\mathbf{v}}_{ij} \cdot \nabla)^2 U
\end{aligned} \tag{B9}$$

$$= -\sum_{j\neq i}^{N} \frac{1}{r_{ij}}\frac{\partial U}{\partial r_{ij}} + \left(\frac{\partial^2 U}{\partial r_{ij}^2} - \frac{1}{r_{ij}}\frac{\partial U}{\partial r_{ij}}\right)(\hat{\mathbf{v}}_{ij} \cdot \hat{\mathbf{r}}_{ij})^2. \tag{B10}$$

For the Lennard-Jones potential the first and second spatial derivatives are given, respectively, by

$$\frac{\partial U}{\partial r_{ij}} = -24\frac{\epsilon}{\sigma}\left[2\left(\frac{\sigma}{r_{ij}}\right)^{13} - \left(\frac{\sigma}{r_{ij}}\right)^{7}\right] \tag{B11}$$

and

$$\frac{\partial^2 U}{\partial r_{ij}^2} = 24\frac{\epsilon}{\sigma^2}\left[26\left(\frac{\sigma}{r_{ij}}\right)^{14} - 7\left(\frac{\sigma}{r_{ij}}\right)^{8}\right]. \tag{B12}$$

The form of $\nabla_{\mathbf{r}_i} \cdot \mathbf{f}_i$ in Eq. (B10) together with Eqs. (B11) and (B12) are the desired expressions needed to perform the NHBTf thermostat simulations (Sec. III).

[1] D. J. Evans and G. Morriss, *Statistical Mechanics of Nonequilibrium Liquids* (Cambridge University Press, Cambridge, 2008).
[2] W. G. Hoover, *Computational Statistical Mechanics* (Elsevier, Amsterdam, 1991).
[3] S. Nosé, Mol. Phys. **52**, 255 (1984).
[4] W. G. Hoover, Phys. Rev. A **31**, 1695 (1985).
[5] P. Hunenberger, Adv. Polym. Sci. **173**, 105 (2005).
[6] A. Bulgac and D. Kusnezov, Phys. Rev. A **42**, 5045 (1990).
[7] G. J. Martyna, M. L. Klein, and M. Tuckerman, J. Chem. Phys. **97**, 2635 (1992).
[8] W. G. Hoover and B. L. Holian, Phys. Lett. A **211**, 253 (1996).
[9] A. C. Brańka, M. Kowalik, and K. W. Wojciechowski, J. Chem. Phys. **119**, 1929 (2003).
[10] A. C. Brańka and K. W. Wojciechowski, Phys. Rev. E **62**, 3281 (2000).
[11] D. J. Evans and G. P. Morriss, Phys. Rev. Lett. **51**, 1776 (1983).
[12] W. G. Hoover, A. J. C. Ladd, and B. Moran, Phys. Rev. Lett. **48**, 1818 (1982).
[13] H. H. Rugh, Phys. Rev. Lett. **78**, 772 (1997).
[14] O. G. Jepps, G. Ayton, and D. J. Evans, Phys. Rev. E **62**, 4757 (2000).
[15] G. Rickayzen and J. G. Powles, J. Chem. Phys. **114**, 4333 (2001).
[16] J. Delhommelle and D. J. Evans, Mol. Phys. **99**, 1825 (2001).
[17] C. Braga and K. P. Travis, J. Chem. Phys. **123**, 134101 (2005).
[18] K. P. Travis and C. Braga, Mol. Phys. **104**, 3735 (2006).
[19] K. P. Travis and C. Braga, J. Chem. Phys. **128**, 014111 (2008).
[20] Wm. G. Hoover and C. G. Hoover, Phys. Rev. E **79**, 046705 (2009).
[21] S. D. Stoyanov and R. D. Groot, J. Chem. Phys. **122**, 114112 (2005).
[22] C. P. Lowe, Europhys. Lett. **47**, 145 (1999).
[23] E. A. J. F. Peters, Europhys. Lett. **66**, 311 (2004).
[24] H. C. Andersen, J. Chem. Phys. **72**, 2384 (1980).
[25] M. P. Allen and F. Schmid, Mol. Simul. **33**, 21 (2007).
[26] K. Meier and S. Kabelac, J. Chem. Phys. **124**, 064104 (2006).
[27] B. L. Holian, A. F. Voter, and R. Ravelo, Phys. Rev. E **52**, 2338 (1995).
[28] G. E. Valenzuela, J. H. Saavedra, R. E. Rozas, and P. G. Toledo, Mol. Simul. **41**, 521 (2015).
[29] S. Nosé, Prog. Theor. Phys. Supp. **103**, 1 (1991).
[30] A. C. Brańka, Phys. Rev. E **61**, 4769 (2000).
[31] J. K. Johnson, J. A. Zollweg, and K. E. Gubbins, Mol. Phys. **78**, 591 (1993).
[32] T. M. Yigzawe and R. J. Sadus, J. Chem. Phys. **138**, 194502 (2013).
[33] J. P. Hansen and I. R. McDonald, *Theory of Simple Liquids* (Academic Press, New York, 2005).
[34] L. V. Woodcock, AIChE J. **52**, 438 (2006).
[35] D. J. Evans and S. Sarman, Phys. Rev. E **48**, 65 (1993).
[36] J. J. Erpenbeck, Phys. Rev. Lett. **52**, 1333 (1984).
[37] D. M. Heyes, J. Chem. Soc. Faraday Trans. II **82**, 1365 (1986).
[38] D. H. Li and J. Jellinek, Z. Phys. D **12**, 177 (1989).
[39] J. Jellinek and D. H. Li, Phys. Rev. Lett. **62**, 241 (1989).
[40] T. Niiyama, Y. Shimizu, T. R. Kobayashi, T. Okushima, and K. S. Ikeda, Phys. Rev. Lett. **99**, 014102 (2007).
[41] T. Niiyama, Y. Shimizu, T. R. Kobayashi, T. Okushima, and K. S. Ikeda, Phys. Rev. E **79**, 051101 (2009).
[42] F. Calvo and P. Labastie, Eur. Phys. J. D **3**, 229 (1998).
[43] S. A. Paz, E. P. M. Leiva, J. Jellinek, and M. M. Mariscal, J. Chem. Phys. **134**, 094701 (2011).
[44] A. C. Brańka and M. Parrinello, Mol. Phys. **58**, 989 (1986).
[45] D. Kusnezov, A. Bulgac, and W. Bauer, Ann. Phys. **204**, 155 (1990).
[46] A. A. Catherall, J. R. Melrose, and R. C. Ball, J. Rheol. **44**, 1 (2000).
[47] J. R. Melrose and R. C. Ball, J. Rheol. **48**, 937 (2004).
[48] J. R. Melrose and R. C. Ball, J. Rheol. **48**, 961 (2004).
[49] F. Calvo and P. Parneix, J. Chem. Phys. **119**, 256 (2003).
[50] R. Angélil, J. Diemand, K. K. Tanaka, and H. Tanaka, J. Chem. Phys. **140**, 074303 (2014).
[51] W. Dzwinel, W. Alda, M. Pogoda, and D. A. Yuen, Physica D **137**, 157 (2000).
[52] M. Mella, J. Chem. Phys. **131**, 124309 (2009).